Adsorption of NH3with Different Coverages on Single-Walled ZnO Nanotube: DFT and QTAIM Study

Adsorption of NH_3 with different coverages on Single-Walled ZnO nanotube: DFT and QTAIM study

Naiara L. Marana,[a] Silvia M. Casassa[b], and Julio R. Sambrano[a]

[a]Modeling and Molecular Simulations Group, São Paulo State University, UNESP, 17033-360, Bauru, SP, Brazil

[b]Theoretical Group of Chemistry, Chemistry Department I.F.M., Torino University, Torino, Italy

Abstract

NH_3 adsorption with different coverages on single-walled (10,10) armchair ZnO nanotube (ZnONT) has been studied via periodic computational simulations at the all-electron B3LYP level. In order to fully characterize the molecules-surface interaction, Infrared (IR) spectrum was calculated for the first time. A rigorous analysis of the electron density in the bonding region, according to the quantum theory of atoms in molecules, was performed. NH_3 molecules physisorb without dissociation via a self-catalyzed process. Although the nanotube undergoes sensitive lattice deformations with low coverages, its fundamental electronic properties were not modified. Owing to these analyses, the armchair nanotubes can be applicable as NH_3 gas sensor.

Graphical abstract

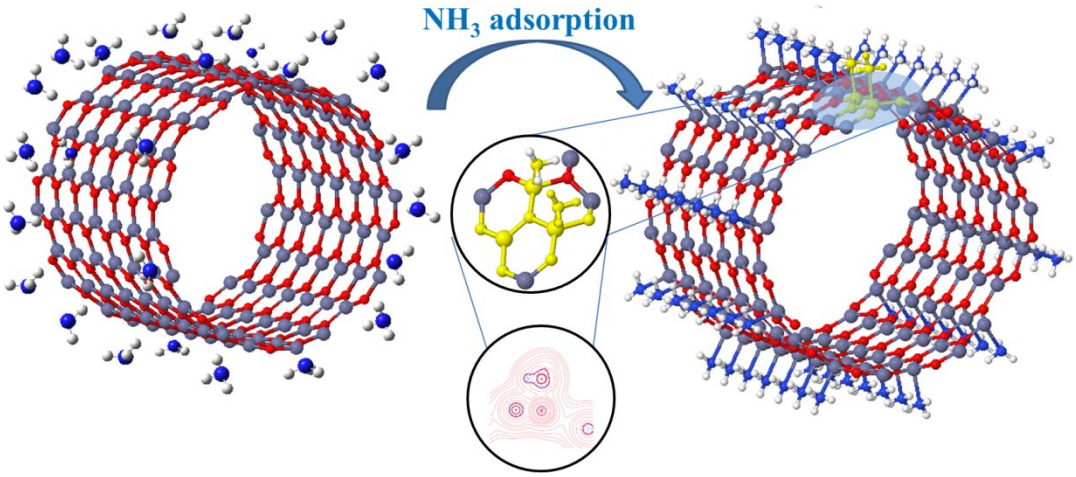

Introduction

Zinc Oxide (ZnO) wurtzite is a well-recognized multifunctional material with a direct band gap energy (3.37 eV)[1] and with several technological applications due to the low cost of synthesis, chemical stability and non-toxicity.[2,3]

In the last years, among other uses, ZnO-based structures applied as gas sensors have been the subject of several research. Catto et. al.[4] reported a low-temperature method to prepare an ozone gas sensor based on hexagonal one-dimensional (1D) ZnO nanorod-like structure via a hydrothermal process. ZnO nanostructures sensitivity towards low O_3 concentrations, as well as good stability, fast response and short recovery time, has been recently reported by Rocha et. al.[5]

An experimental study by Biasotto and co-workers[6] exploited the considerable surface-to-volume ratio and porous sensitivity of ZnO films to design devices for CO gas detection. Wang and co-workers,[7] studied the response and viability of ZnO nanorod to detected NO_2 in presence of several critical influencing factors, have found rather good performances in sensitivity and response speed. ZnO nanorods-based ammonia sensors, with a cross-linked configuration structures, as reported by Chen et. al.,[8] exhibit effective capability in detecting ammonia concentration of 10 ppm NH_3/air.

Due to its high specific area, fine particle size, and quantum confinement properties, ZnO nanowires are believed to represent promising candidates for gas sensing applications[9] in particular as regards to ammonia detection.[10]

On the other hand, a few theoretical papers are devoted to study the characteristics and implications of gas molecules interaction with 1D ZnO structures. An et. al.[11] investigated the electronic and structural properties of a single-walled ZnO nanotube (6, 0) as a potential sensor for O_2, H_2, NH_3, and NO_2. Their density functional theory (DFT) calculations showed that molecules are mainly chemisorbed and that CO and ammonia behaves as charge donors enhancing the electron concentration of ZnO.

Among several gaseous molecules, the present study focus is on ammonia (NH_3) adsorption. This molecule is extensively applied in many areas, such as, food, pharmaceutical and chemical industries, besides medical diagnosis, and others. Nevertheless, ammonia is a toxic gas and a severe irritant to the respiratory tract. An exposure over 15 min needs to be limited to 25–35 ppm and the Time-Weighted-

Average over an 8-h period should not exceed 25 ppm. Depending on those conditions and sensibilities, the critical need of reliable and effective ammonia monitoring everywhere is urgent,[12] which implies the need to develop more efficient materials for detection.

Many ammonia sensors are already based on pure ZnO bulk phases and surfaces.[13-15] Nonetheless, ZnO nanostructures could represent an improvement in gas sensor technology due to their large specific surface area.

This paper reports DFT periodic simulations performed at the B3LYP hybrid functional/all-electron basis set level to investigate the structural and electronic properties of NH_3 adsorption on armchair (10, 10) single-walled ZnO nanotube (*n*NH3@ZnONT). Adsorption energies as a function of the surface coverage are calculated and the influence of the NH_3 adsorption on structural and electronic properties of ZnONT is analyzed. In order to fully characterize the molecules-surface interaction, Infrared (IR) spectra were calculated and a rigorous analysis of the electron density in the bonding region, according to the quantum theory of atoms in molecules (QTAIM)[16] was accomplished.

Theoretical Methods

The computational simulations were performed using the CRYSTAL14[17] program which solves the Schrodinger equation for periodic systems in 1, 2 and 3 dimensions in a basis set of localized atomic orbitals. As the majority of the available studies of our research group[18-20] this paper is based on DFT calculations with the standard B3LYP hybrid functional.[21-23] Zinc, oxygen, nitrogen and hydrogen atoms were described by 86-411d31G[24], 8-411d1[25], 6-21G*[26] and 5-11G*[27] all-electron basis set, respectively. The accuracy of the truncation criteria for bi-electronic integrals is controlled by a set of five thresholds whose values have been set to: 10^{-10}, 10^{-10}, 10^{-10}, 10^{-20}, 10^{-40}. In the self-consistent field procedure (SCF) the shrinking factor for both the Fock matrix diagonalization and the energy calculation was set to 4, corresponding to 3 independent k-points in the irreducible part of the Brillouin zone. Basins integration to estimate atomic Bader charges was performed on a 120x96x120 grid of points in the direct space.[28] The vibrational frequencies at the Γ point were computed within the harmonic approximation by diagonalizing the mass-weighted Hessian matrix.[29,30]

The following step-by-step strategy has been adopted to simulate NH_3 adsorption on ZnONT. First, the wurtzite ZnO bulk structure has been optimized relaxing both the lattice parameters (*a* and *c*) and internal coordinate, *u*. Then, the (0001) monolayer was cut out from the bulk and a new optimization of the internal coordinates of the (0001) surface was performed. Finally, by rolling the (0001) relaxed monolayer surface[17,23,31-33] it was obtained the 40 atoms unit cell (10, 10) armchair nanotube characterized by a diameter of ~18 Å. In a previous works,[32, 33] this structure was designed as an ideal model to perform adsorption studies thanks to its minimum energy formation and strain.

In DFT simulation, in absence of any dynamic and thermal effects, the final configuration of an adsorbate is significantly influenced by its initial position. In order to explore all the possibilities and to individuate both the adsorption sites and the optimum coverage, several different starting configurations were investigated. With reference to Figure 1, four adsorption sites were considered on the ZnONT surface: the axial and equatorial position of Zn (1a-1 and 1a-2) and O atom (1a-3 and 1a-4) respectively. For each adsorption sites, two different molecular approaches were performed: via nitrogen atom (1a-1 and 1a-2) and via hydrogen atom (1a-3 and 1a-4). It

is important to emphasize that the periodicity along one direction is preserved, so all the configurations represents the adsorption of an infinite row of NH_3 molecules along the ZnO *x*-direction (see Figure 2) and this corresponds to one NH_3 per unit cell. To model the single molecule dilution limit a supercell calculation was carried out on a unit containing 160 surface atoms and only 2 NH_3 molecules.

As the equilibrium configuration of a single row of NH_3 was identified, it was considered the possibility of ammonia molecules adsorbed in neighboring positions and then three possibilities were envisaged: both molecules on equatorial (Figure 1b-5) or axial sites (Figure 1b-7) or one ammonia in the axial and the other in the equatorial position (Figure 1b-6). The most stable among these geometries was repeated with NH_3 rows going from 2 up to the saturation limit of 10, as represented in Figure 2.

The adsorption energy was calculated according to the expression:

$$E_{ads/N} = \frac{1}{N}\left[E_{(10,10)+NH_3} - \left(E_{(10,10)} + N\,E_{NH_3}\right) + E_{BSSE}\right] \qquad (1)$$

where $E_{(10,10)+NH_3}$ is the total energy of the optimized (10, 10) nanotube with adsorbed NH_3 molecule, $E_{(10,10)}$ is the total energy of the isolated optimized (10, 10) nanotube, *n* is the number of adsorbed NH_3 molecules per unit cell and E_{NH_3} is the total energy of ammonia in gas phase. E_{BSSE} is the correction energy due to the basis set superposition error (BSSE).[34] Calculations performed with localized basis sets are susceptible to this error, which occurs when atoms belonging to different interacting moieties approach each other and the overlap among their basis functions produces a spurious stabilization, and that is inversely proportional to the quality of the adopted basis set. There are two ways to estimate the BSSE, the *a priori* chemical Hamiltonian approach (CHA)[35] and the *a posteriori* counterpoise method (CP)[34] but, although conceptually different, the two approaches tend to give similar results. In this work, the CP correction was applied to all the energies as follows:

$$E_{BSSE} = \left(E^{frozen}_{(10,10)} - E^{frozen}_{(10,10)+ghost}\right) + \left(E^{frozen}_{NH_3} - E^{frozen}_{ghost+NH_3}\right) \qquad (2)$$

where all the energies refer to the geometries of the two separated moieties *frozen* in the minimum adsorption configuration, with and without ghost functions, respectively.

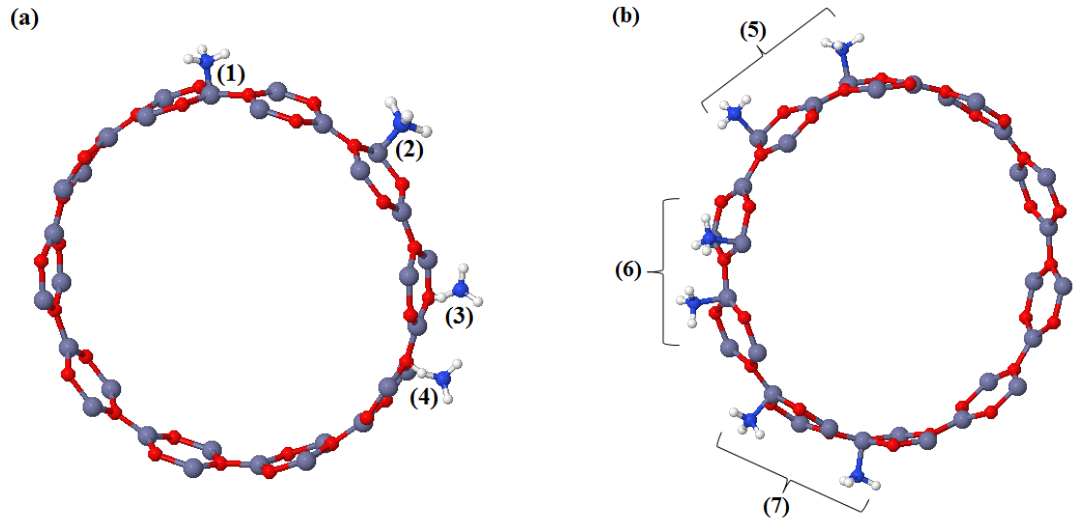

Figure 1: NH_3 adsorption on various surface sites and with different coverages (a) (1) Model A – Zn_{Ax}-NH_3, (2) Model B – Zn_{Eq}-NH_3, (3) Model C – O-HNH_2, (4) Model D – O-HNH_2, and simultaneous adsorption (b) (5) both Zn_{Eq}, (6) Zn_{Eq} and Zn_{Ax}, and (7) both Zn_{Ax}

The distortion energy, E_{dist}, due to the structural modifications of the ZnONT lattice, that occur as one of the main effect of the adsorption process, was evaluated according to the following equation:

$$E_{dist/N} = \frac{1}{N}\left(E_{(10,10)}^{frozen} - E_{(10,10)}\right) \quad (3)$$

In order to estimate the heat of adsorption and its temperature dependency, the enthalpy of each moiety was calculated at 0 and 298 K as follows:

$$H(T) = E_L + E_0 + PV + E_T \quad (4)$$

where E_L is the electronic term, E_0 and E_T are the zero-point and temperature dependent contributions to the vibrational energy, respectively and PV is the pressure per volume contribution.

Finally, the ZnONT-NH_3 interactions was characterized by exploiting the potentiality of Bader topological analysis of the electron density, as implemented in the TOPOND program[28] incorporated in the CRYSTAL14 package. Bader charges were computed to estimate the amount and direction of the charge transfer between the NH_3

and the ZnONT. A complete search of the bond critical points (BCP) between the adsorbates and the nanotube has been carried out and their topology has been fully characterized to shed light on the bonding nature. Moreover, the sensitiveness of these indicators has allowed us to follow the effects of the adsorption and coverage on the Zn-O bonds.

Results and discussion

Previous accurate studies on the structural, electronic and vibrational properties of ZnO bulk, (0001) monolayer surface and bare armchair nanotube can be found in References 32 and 33. Ammonia adsorption has then been modeled on the fully characterized ZnONT surface.

On the basis of preliminary investigation on the four different sites, it was confirmed that NH_3 adsorption takes place via nitrogen on Zn atom in the axial position. The overall energy cost, which takes into account both the N-Zn bond formation and the nanotube relaxation, is about 8.0 and 15.0 kcal/mol lower than that on the others sites, whose optimized geometries are reported in the Supplemental material, Figure S1.

The results are summarized in Table 1, the adsorption occurring via nitrogen on the Zn axial atoms and characterized by an equilibrium distance of 2.30 Å. The adsorption energy of NH_3 calculated with the supercell approach (2 NH_3 per 160 atoms) is -4.46 kcal/mol and represents our model for isolated ammonia interacting with ZnONT. As far as a single row of NH_3 is considered, the binding energy increases and the difference between this two values, about 1 kcal/mol, is a good estimate of the hydrogen-bonds which takes place between nearby adsorbed molecules. For what concerns the adsorption geometry, NH_3 almost preserves its gas phase structure and, regardless of NH_3 concentration, its protons point far from the surface and do not interact with the underlying oxygen atoms. On the contrary, the surface atoms involved in the process show a sensitive elongation of their bond length and shrinkage of the angles. Oxygen and Zn atoms belonging to the other hexagons are almost unaffected by NH_3 uptake indicating that the interaction is rather localized although effective. In fact, the values of E_{dist} are not negligible with a maximum strain suffered by the *2*NH_3@ZnONT system, which is visibly stretched along the Zn-NH_3 direction and a minimum for the symmetric *10*NH_3@ZnONT coverage.

As a general comment, our adsorption energies are sensitively lower than those evaluated by others authors on similar systems.[11,36-39] Indeed are many reasons to explain these differences. First, most of the calculated binding energies do not take into account the BSSE. Our CP correction is in the order of 9.0 kcal/mol, a value that, if neglected, would yield results in better agreement with literature. Then, as regard the only other adsorption studied on nanotube,[11] zigzag (6,0) is demonstrated to be a rather

instable structure[33] and this can enhance its reactivity. Moreover, in literature it was modeled the adsorption of a single NH_3 on a surface and the effects of different coverage were not taken into account. Then, as can be seen in Figure 2 and already commented, the interaction with ammonia induces evident deformations on the soft nanotube lattice, estimated to be in the order of 3-5 kcal/mol, strains that are totally absent in the case of extended surfaces. Finally, some surfaces present a complete different topology and this is the case of the $(10\bar{1}0)$ layer where both the Zn and the O atoms are exposed and can easily interact with the incoming molecule.

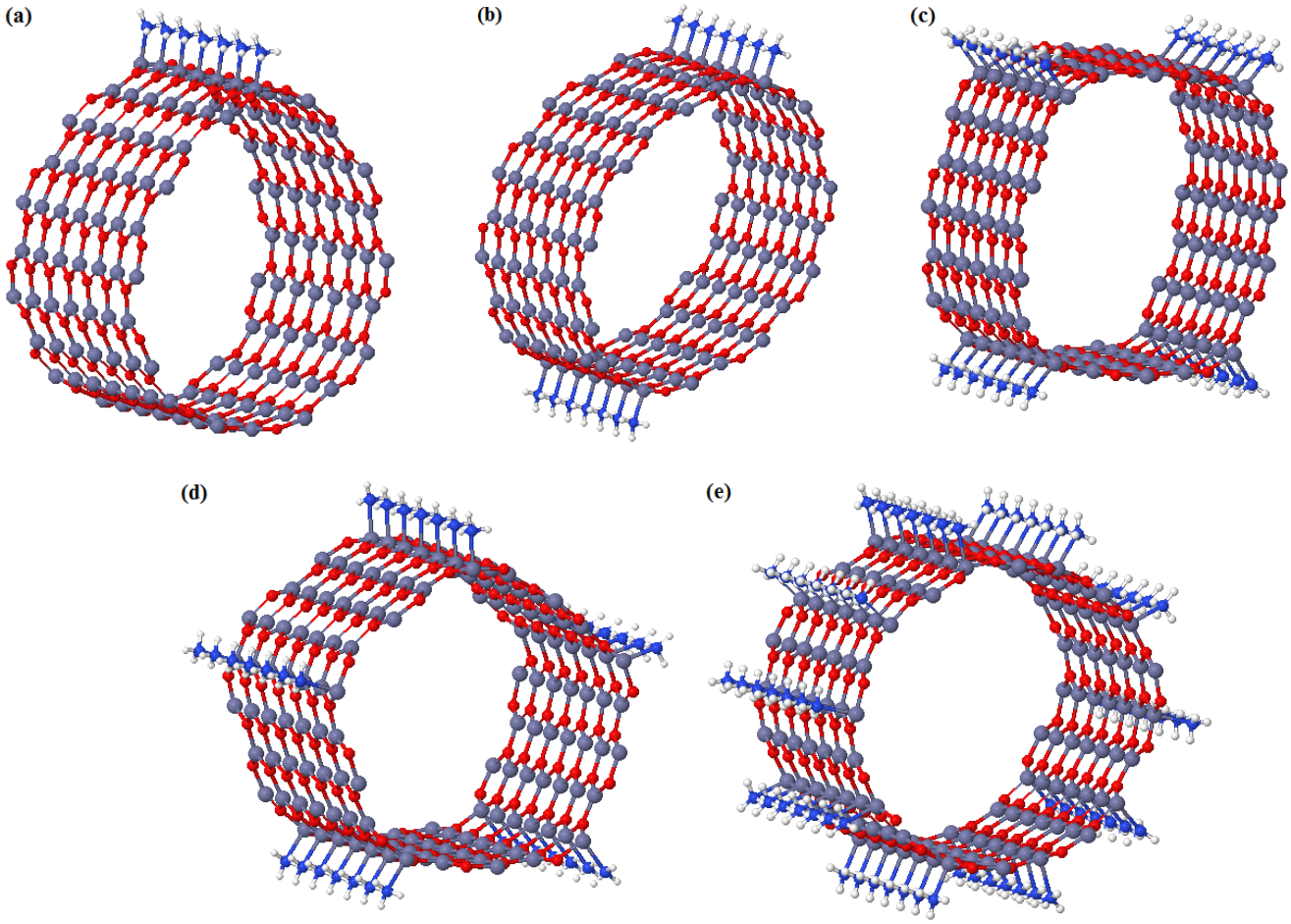

Figure 2: Nanotube deformation after NH_3 adsorption and optimization (a) 1-row of NH_3 molecules, (b) 2-rows (c) 4-rows NH_3, (d) 5-rows and (e) 10-rows.

Table 1: Zn-O, N-H, and Zn-N bond lengths (Å), Zn-O-Zn and H-N-H bond angles (degree) distortion energy (E_{dist}) and adsorption energy (E_{ads}) in kcal/mol and band gap ($E_{gap,}$ eV) of *n*NH3@ZnONT. The sub-index *s* refers to the atoms of the adsorption site.

nNH$_3$	d_{Zn-O}	$d_{s(Zn-O)}$	$\alpha_{Zn-O-Zn}$	$\alpha_{sZn-O-Zn}$	d_{Zn-N}	d_{N-H}	α_{H-N-H}	E_{dist}	E_{ads}	$E_{ads}+E_{BSSE}$	E_{gap}
0	1.89	1.89	119.79	119.79	-	-	-	-	-	-	4.52
1	1.89	1.93	119.88	116.12	2.32	1.02	107.49	3.35	-16.77	-4.46	4.18
1-row	1.91	1.94	119.74	117.88	2.32	1.02	103.02	2.45	-9.70	-5.46	4.36
2-row	1.90	1.94	119.64	117.87	2.30	1.02	107.35	5.39	-14.38	-4.95	4.43
4-row	1.90	1.94	119.87	118.17	2.31	1.02	107.30	3.72	-15.79	-6.43	4.38
5-row	1.90	1.94	119.90	118.28	2.33	1.02	106.40	3.50	-15.84	-6.48	4.37
10-row	1.90	1.93	119.90	118.93	2.37	1.02	106.33	2.14	-15.46	-6.31	4.22
6 (6, 0)[11]	1.94	-	-	-	2.16	-	-	-	-18.86	-	2.25
1 (0001)[37]	-	-	-	-	2.04	-	-	-	-51.00	-	-
1 (10$\bar{1}$0)[36]	-	-	-	-	2.06	1.02	107.00	-	-35.00	-	-
1 (10$\bar{1}$0)[39]	-	-	-	-	2.06	1.01	-	-	-42.02	-	-

In order to take into account the effect of the nuclear motion on the surface processes, the heats of adsorption were calculated, at 0 and 298 K, and reported in Table 2. In the entire range of concentration explored, NH_3 physisorption occurs as an exothermic process only slightly affected by an increase of the temperature.

Table 2: Adsorption energies and enthalpy at 0 and 298 K in kcal/mol

nNH$_3$	$E_{ads}+E_{BSSE}$	H_{ads} (0K)	H_{ads} (298K)
1-row	-5.46	-3.30	-2.84
4-row	-6.43	-4.30	-4.21
10-row	-6.31	-4.31	-4.28

With regards to the electronic structure, it can be observed that the calculated energy gaps, E_{gap}, decreases with the formation of the coating layer of NH_3 but the semiconductor character of ZnONT is preserved in all cases.

With the aim of the investigation the electronic structure of these heterogeneous systems, the bands structure and density of states of *10*NH$_3$@ZnONT with bare nanotube were compared. As can be seen in Figure S3 the physisorption keeps the bands main features unchanged. On the contrary, as already said, some effects can be perceived on the band gap which undergoes a small but sensitive reduction due to the upper shift of the occupied 3*d* orbitals of the Zn atom. In particular, the $3d_{(x^2-y^2)}$ and $3d_{xy}$ orbitals are shifted higher in energy with respect to the others, see Figure 3. At the conduct band, ~9.0 eV, the *p* orbitals of zinc atoms maintain the contribution while the

$2p$ orbitals of oxygen atoms decrease the contribution after adsorption. With respect to the NH_3 molecules, the contribution of nitrogen is most intense in the valence band, while the hydrogen contributes more in the conduction band. The orbital $2p_xp_y$ of nitrogen atoms contribute more over the entire range examined, the s and $2p_z$ orbitals presents almost the same contribution.

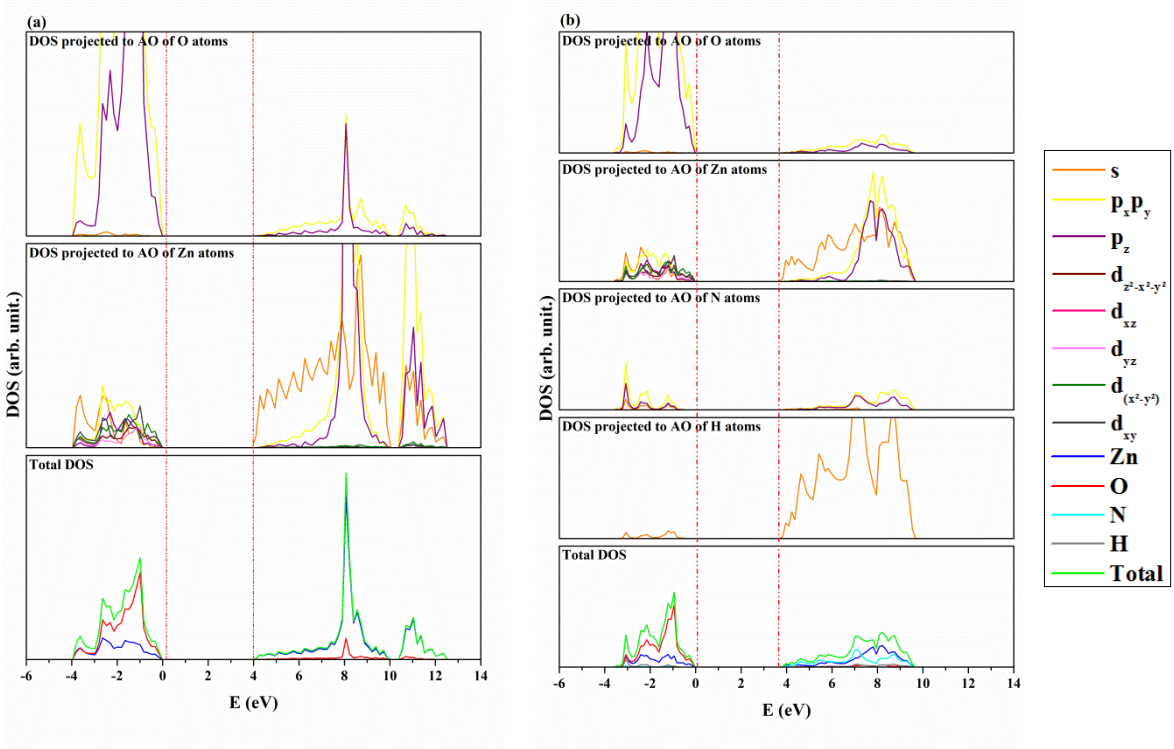

Figure 3: Density of states (a) bare (10, 10) nanotube and (b) with 10-rows of NH_3 molecules adsorbed.

IR spectra of *10*NH3@ZnONT, calculated in the whole energy range, is subdivided for sake of clarity into two parts, the low (0-900 cm^{-1}) and high (900-3600 cm^{-1}) frequencies regions, reported in Figure 4a and 4b, respectively. Signals of the isolated ZnONT and of the gas phase NH_3 molecule are superimposed, for sake of comparison.

Nanotube vibrates according to modes with frequencies below 700 cm^{-1}. As the adsorption takes place, peaks between 546-553 cm^{-1}, mainly due to oxygen displacements,[33] are split in several signals. Then, a low intensity peak rises up at 187-193 cm^{-1} and is assigned to the stretching of the Zn-N bond (Figure 4c).

Above 700 cm^{-1} ZnONT is silent and the signals due to N-H bonds can be accurately detected. The frequencies calculated for the NH_3 isolated molecule are 1226, 1720 (bending), 3340 and 3443 cm^{-1}(stretching) and result in good agreement with both experimental values[40] and recently computed modes.[41] After adsorption, the two signals at high-frequency remain almost unchanged, as expected. On the contrary, the soft bending modes active at lower frequencies, which yield the molecule closer to the ZnONT surface, are lowered and split in few clear signals emerging in the region around 1170 and 1700 cm^{-1}, respectively.

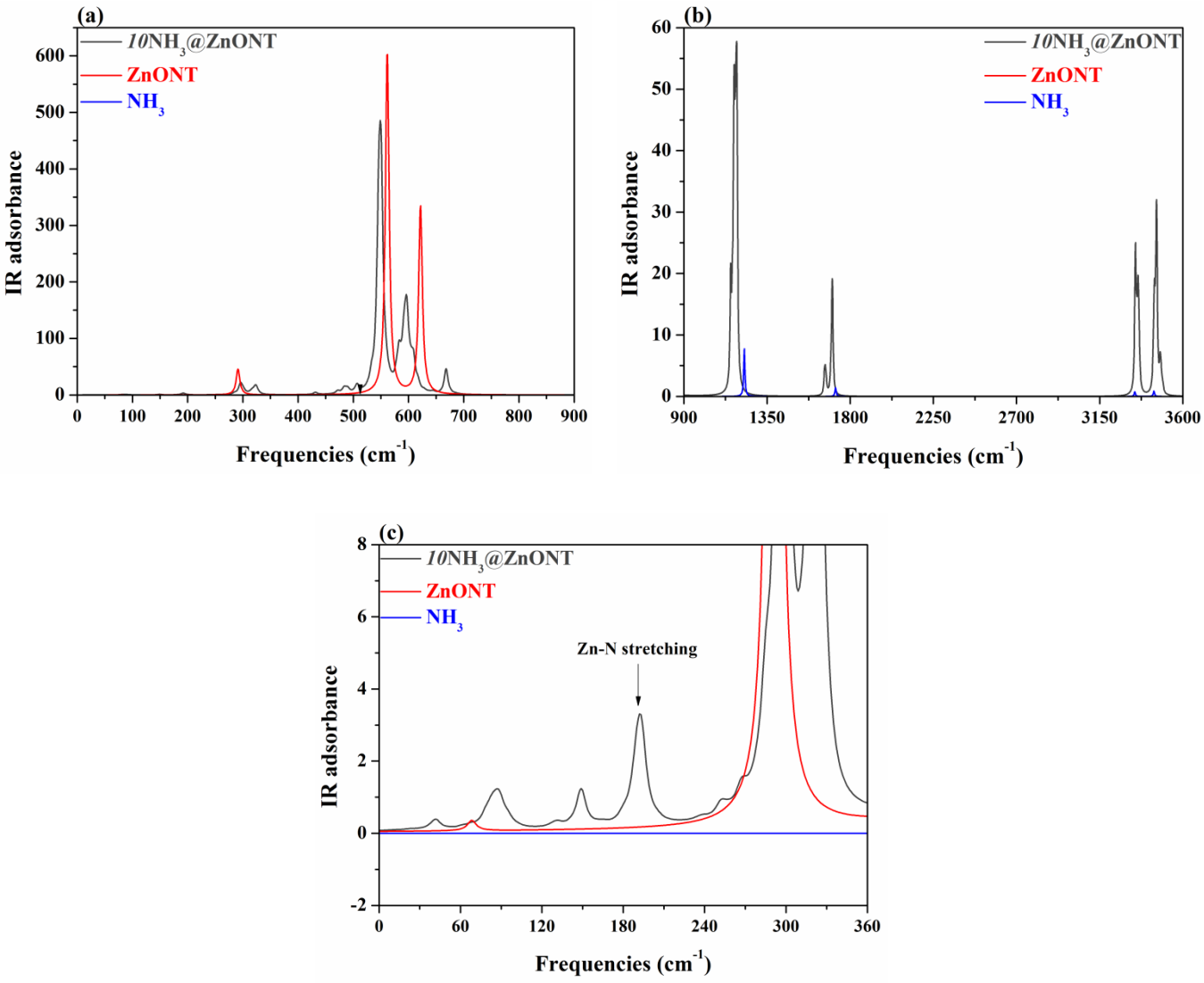

Figure 4: Infrared spectra of NH_3 adsorption on ZnONT in the low (a) and high (b) frequency range. In (c) a zoom of the peaks corresponding to the Zn-N stretching modes.

Finally, the topological analysis of the electron density was performed with particular attention to the atoms involved in the ZnONT-NH_3 interaction, represented, for sake of clarity, in the inset of Figure 5. Results, in terms of bond critical points (BCP) their topological properties and charge densities are collected in Table 3. On the basis of the topological indicators[42] a tentative classification of the various interaction is proposed. The Zn-O bond, as already studied,[33] can be seen as a transit (*t*) interaction, neither ionic either covalent. In the transit region can also be placed the Zn-N bond: the driving force in this case seems to be the electrostatic interaction between NH_3 permanent dipole moment with the Zn Lewis acid site. The value of the dipole moment increases as NH_3 approaches the nanotube as demonstrated by the remarkable charge transfer from the protons to the nitrogen. On the contrary, not appreciable charge transfer is calculated between the two interacting moieties, in particular Zn and O atoms keep both their volume and charge, after the adsorption. Finally hydrogen-bonds between NH_3 molecules along the same row are formed, one proton of each molecule pointing towards the N of the opposite ammonia and these interactions stabilize the whole structure.

In Figure 6 the total electron density and its Laplacian are shown, in the plane containing the Zn-N bond. ZnO charge density is not significantly altered by the adsorption, whereas its geometrical structures is very responsive, on the contrary, NH_3 molecules retain almost the same geometry as in the gas phase but undergoes to sensitive changes in their electronic features.

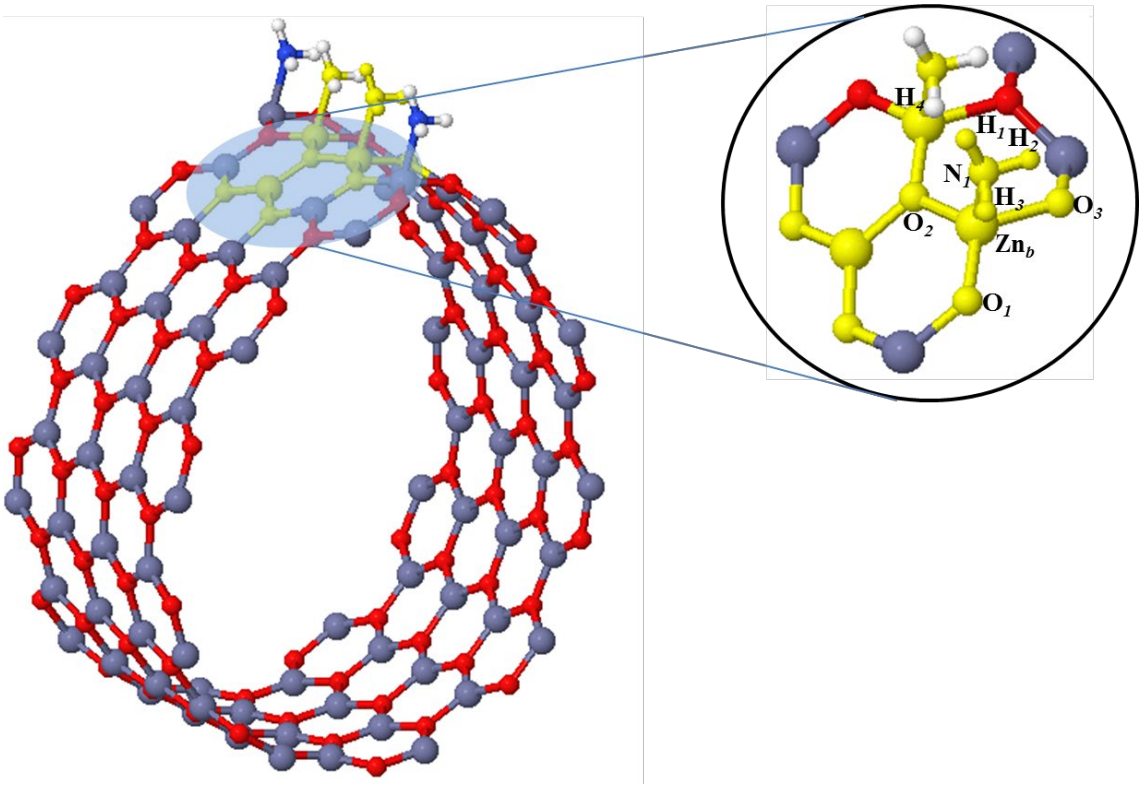

Figure 5: ZnO nanotube with NH_3 molecules adsorbed. In yellow, the atoms that were considered for the topological analysis in Table 3

Table 3: Topological properties at the bond critical points (electron charge density ($\rho(r)$), Laplacian ($\nabla^2\rho$), |V|/G ratio, bond degree H/ρ(r), ellipticity ε) plus Bader charges and atomic volumes (all in atomic units) are computed for the atoms involved in the physisorption (labels of atoms as in Figure 5). Subindex *f* refers to the isolated nanotube and NH_3; *t*, *cov* and *H-bond* refers to the transit, covalent and hydrogen bond type

	Bond Critical Points								**Atomic Properties**	
	$\mathbf{d_{BCP-Zn/N}}$	$\mathbf{d_{BCP-O/H}}$	$\boldsymbol{\rho(r)}$	$\boldsymbol{\nabla^2\rho}$	|V|/G	H/$\rho(r)$	ε	*bond*	Q	V
Zn_f									1.27	79.80
O_{in}	0.919	0.970	0.098	0.571	1.06	-0.09	0.028	*t*	-1.12	112.67
O_{out}	0.920	0.971	0.090	0.508	1.05	-0.08	0.028	*t*	-1.20	111.58
N_f									-0.84	94.36
H_f	0.747	0.279	0.320	-1.359	8.36	-1.23	0.037	*cov*	0.28	38.83
1-row NH_3										
Zn_b									1.29	78.93
O_1	0.922	0.975	0.098	0.573	1.06	-0.09	0.026	*t*	-1.11	111.82
O_2	0.972	0.983	0.095	0.551	1.06	-0.09	0.025	*t*	-1.19	111.38
O_3	0.941	1.004	0.088	0.489	1.05	-0.08	0.011	*t*	-1.04	108.96
N_1	1.104	1.197	0.043	0.121	1.23	-0.21	0.034	*t*	-1.08	111.84
N_1									-1.08	112.83
H_1	0.748	0.279	0.323	-1.413	9.01	-1.25	0.028	*cov*	0.34	32.40
H_2	0.756	0.267	0.323	-1.454	9.73	-1.27	0.027	*cov*	0.38	29.90
H_3	0.760	0.263	0.323	-1.472	9.97	-1.28	0.025	*cov*	0.40	23.11
H_4	1.479	0.880	0.013	0.045	0.91	0.07	0.193	*H-bond*	0.38	37.71
10-row NH_3										
Zn_b									1.29	80.58
O_1	0.928	0.984	0.094	0.547	1.06	-0.09	0.021	*t*	-1.12	112.94
O_2	0.923	0.976	0.097	0.569	1.06	-0,09	0,023	*t*	-1.20	111.38
O_3	0.936	0.997	0.090	0.509	1.05	-0.08	0.013	*t*	-1.04	108.98
N_1	1.146	1.236	0.036	0.095	1.25	-0.22	0.041	*t*	-1.08	114.03
N_1									-1.08	114.03
H_1	0.746	0.276	0.323	1.391	8.71	-1.24	0.030	*cov*	0.33	33.44
H_2	0.762	0.264	0.321	1.457	9.94	-1.28	0.026	*cov*	0.40	23.36
H_3	0.755	0.268	0.323	1.440	9.52	-1.26	0.028	*cov*	0.37	30.51
H_4	1.495	0.892	0.013	0.043	0.91	0.07	0.156	*H-bond*	0.36	38.26

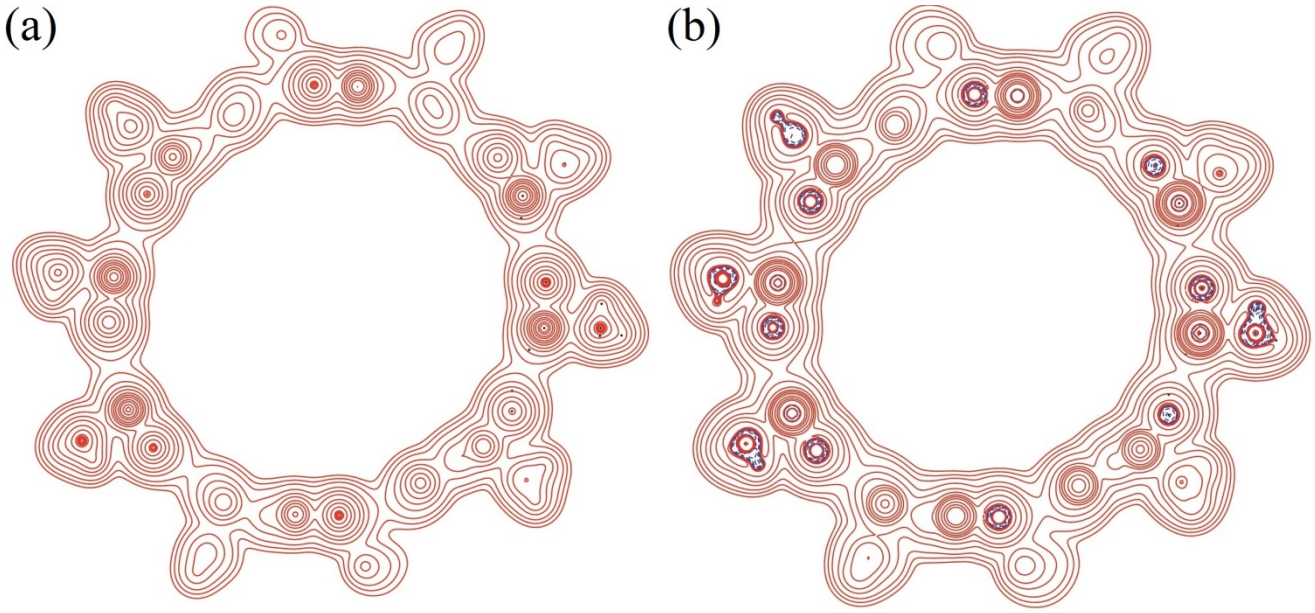

Figure 06: (a) Electron density and (b) Laplacian of the electron density in the plane containing the N-Zn-O atoms evaluated at the B3LYP level. A logarithmic scale is adopted between -0.1 and 0.1 au. Continuous red and dotted blue lines indicate positive and negative contour levels, respectively.

On the basis of our results, it is possible to affirm that, in presence of a continuous source of NH_3, the adsorption can proceed until complete coverage of the Zn atoms. Ammonia uptake induces in the ZnONT structural modifications which, however, do not change the fundamental electronic structure and the overall process is self-catalyzed thanks to the formation of attractive interactions between the adsorbed molecules.

Conclusions

Periodic DFT calculations with B3LYP and all-electron Gaussian basis set were performed to simulate the structural, electronic, vibrational and topological properties of armchair ZnONT as ammonia gas sensor through the NH_3 adsorption at nanotube external surface. The analysis of total energy of the system showed that the NH_3 is adsorbed on Zn at axial position, and the interaction between the polar molecule and the basic site plays a leading role in determining the adsorption energy of the system.

As expected in physisorption, the band structure of the host ZnONT system is practically unchanged and only few differences in the Zn atoms 3*d* orbitals contributing to the valence bands were appreciated. NH_3-ZnONT interaction produces its traces in the IR spectrum where Zn-N vibrational modes appear around 187 cm^{-1} and the frequencies of the isolated systems are perturbed by the adsorption. The onset of a Zn-N interaction and the formation of $N \cdots H$ hydrogen-bond were also confirmed by the topological analysis of the electron density.

With an increase of molecules adsorbed, the deformation at nanotube structure decreases, weak attractive interactions between physisorbed molecules are evaluated and then it can be concluded that, in a real system, the molecules trend to saturated the surface and not change significantly the nanotube structure or the semiconductor character, as the energy band gap is preserved.

Owing to these analyses, the armchair nanotube can be used as ammonia gas sensor without any modification on its structure or properties.

Supporting Information

Models of adsorption site, single molecule adsorption, and band structure of bare nanotube and saturated nanotube.

Acknowledgments

This work is supported by Brazilian Funding Agencies: CNPq, CAPES, FAPESP (2013/19713-7, 2013/07296-2, 2016/07954-8, 2016/07476-9). The computational facilities were supported by resources supplied by Molecular Simulations Laboratory, São Paulo State University, Bauru, Brazil.

References

1. Reynolds, D. C.; Look, D. C.; Jogai, B. Optically pumped ultraviolet lasing from ZnO. *Solid State Commun.* **1996,** *99*, 873-875.
2. Ozgur, U.; Hofstetter, D.; Morkoc, H. ZnO Devices and Applications: A Review of Current Status and Future Prospects. *Proceedings of the Ieee.* **2010,** *98*, 1255-1268.
3. Morkoç, H.; Özgür, Ü. *Zinc Oxide: Fundamentals, Materials and Device Technology*; Wiley-VHC: Federal Republic of Germany, DEU, 2009.
4. Catto, A. C.; da Silva, L. F.; Ribeiro, C.; Bernardini, S.; Aguir, K.; Longo, E.; Mastelaro, V. R. An easy method of preparing ozone gas sensors based on ZnO nanorods. *Rsc Advances.* **2015,** *5*, 19528-19533.
5. Rocha, L. S. R.; Foschini, C. R.; Silva, C. C.; Longo, E.; Simoes, A. Z. Novel ozone gas sensor based on ZnO nanostructures grown by the microwave-assisted hydrothermal route. *Ceram. Int.* **2016,** *42*, 4539-4545.
6. Biasotto, G.; Ranieri, M. G. A.; Foschini, C. R.; Simoes, A. Z.; Longo, E.; Zaghete, M. A. Gas sensor applications of zinc oxide thin film grown by the polymeric precursor method. *Ceram. Int.* **2014,** *40*, 14991-14996.
7. Wang, X. M.; Sun, F. Z.; Duan, Y. Q.; Yin, Z. P.; Luo, W.; Huang, Y. A.; Chen, J. K. Highly sensitive, temperature-dependent gas sensor based on hierarchical ZnO nanorod arrays. *J. Mater. Chem. C.* **2015,** *3*, 11397-11405.
8. Chen, T.-Y.; Chen, H.-I.; Hsu, C.-S.; Huang, C.-C.; Wu, J.-S.; Chou, P.-C.; Liu, W.-C. Characteristics of ZnO nanorods-based ammonia gas sensors with a cross-linked configuration. *Sens. Actuators, B.* **2015,** *221*, 491-498.
9. Wan, Q.; Li, Q. H.; Chen, Y. J.; Wang, T. H.; He, X. L.; Li, J. P.; Lin, C. L. Fabrication and ethanol sensing characteristics of ZnO nanowire gas sensors. *Appl. Phys. Lett.* **2004,** *84*, 3654-3656.
10. Wang, X. H.; Zhang, J.; Zhu, Z. Q. Ammonia sensing characteristics of ZnO nanowires studied by quartz crystal microbalance. *Appl. Surf. Sci.* **2006,** *252*, 2404-2411.
11. An, W.; Wu, X.; Zeng, X. C., Adsorption of O-2, H-2, CO, NH3, and NO2 on ZnO nanotube: A density functional theory study. *J. Phys. Chem. C.* **2008,** *112*, 5747-5755.
12. Gangopadhyay, R. K.; Das, S. K. Ammonia leakage from refrigeration plant and the management practice. *Process Saf. Prog.* **2008,** *27*, 15-20.
13. Saito, S.; Miyayama, M.; Koumoto, K.; Yanagida, H. Gas sensing characteristic of porous ZnO and Pt/ZnO ceramics. *J. Am. Ceram. Soc.* **1985,** *68*, 40-43.
14. Nanto, H.; Minami, T.; Takata, S. Zinc-oxide thin-film ammonia gas sensors with high-sensitivity and excellent selectivity. *J. Appl. Phys.* **1986,** *60*, 482-484.
15. Aslam, M.; Chaudhary, V. A.; Mulla, I. S.; Sainkar, S. R.; Mandale, A. B.; Belhekar, A. A.; Vijayamohanan, K. A highly selective ammonia gas sensor using surface-ruthenated zinc oxide. *Sens. Actuators, A.* **1999,** *75*, 162-167.
16. Bader, R. F. W. *Atoms in Molecules - A Quantum Theory;* Oxford University Press: Oxford, U. K., 1990.
17. Dovesi, R.; Orlando, R.; Erba, A.; Zicovich-Wilson, C. M.; Civalleri, B.; Casassa, S.; Maschio, L.; Ferrabone, M.; De La Pierre, M.; D'Arco, P.; et. al. CRYSTAL14: A Program for the Ab Initio Investigation of Crystalline Solids. *Int. J. Quantum Chem.* **2014,** *114*, 1287-1317.
18. Maul, J.; Santos, I. M. G.; Sambrano, J. R.; Erba, A. Thermal properties of the orthorhombic CaSnO3 perovskite under pressure from ab initio quasi-harmonic calculations. *Theor. Chem. Acc.* **2016,** *135:36,* 1-9.
19. Albuquerque, A. R.; Maul, J.; Longo, E.; dos Santos, I. M. G.; Sambrano, J. R. Hydrostatic and 001 Uniaxial Pressure on Anatase TiO2 by Periodic B3LYP-D* Calculations. *J. Phys. Chem. C.* **2013,** *117*, 7050-7061.

20. Duarte, T. M.; Buzolin, P. G. C.; Santos, I. M. G.; Longo, E.; Sambrano, J. R. Choice of hybrid functional and basis set optimization to calculate the structural, electronic, mechanical, and vibrational properties of BaSnO3. *Theor. Chem. Acc.* **2016**, *135:151,* 1-8.
21. Becke, A. D. Density-functional Thermochemistry .3. The Role of Exact Exchange. *J. Chem. Phys.* **1993,** *98,* 5648-5652.
22. Lee, C. T.; Yang, W. T.; Parr, R. G. Development of the colle-salvetti correlation-energy formla into a functional of the electron-density. *Phys. Rev. B: Condens. Matter.* **1988,** *37*, 785-789.
23. Dovesi, R.; Roetti, C.; Orlando, R.; Zicovich-Wilson, C. M.; Pascale, F.; Civalleri, B.; Doll, K.; Harrison, N. M.; Bush, I. J.; D'Arco, P.; et. al. CRYSTAL14 User's Manual: University of Torino, Torino, ITA, 2014.
24. Jaffe, J. E.; Hess, A. C. Hartree-Fock study of Phase-changes in ZnO at High-pressure. *Phys. Rev. B: Condens. Matter.* **1993,** *48*, 7903-7909.
25. Bredow, T.; Jug, K.; Evarestov, R. A. Electronic and magnetic structure of ScMnO3. *Phys. Status Solidi B.* **2006,** *243*, R10-R12.
26. Dovesi, R.; Causa, M.; Orlando, R.; Roetti, C.; Saunders, V. R. Abinitio approach to molecular-crystals - A periodic Hartree-Fock study of crystalline urea. *J. Chem. Phys.* **1990,** *92*, 7402-7411.
27. Dovesi, R.; Ermondi, E.; Ferrero, E.; Pisani, C.; Roetti, C. Hartree-Fock study of lithium hydride with the use of a polarizable basis set. *J. Phys. Rev. B.* **1983,** *29*, 3591-3600.
28. Gatti, C.; Casassa, S. TOPOND user's manual; Millano, ITA, 2013.
29. Pascale, F.; Zicovich-Wilson, C. M.; Gejo, F. L.; Civalleri, B.; Orlando, R.; Dovesi, R. The calculation of the vibrational frequencies of crystalline compounds and its implementation in the CRYSTAL code. *J. Comput. Chem.* **2004,** *25*, 888-897.
30. Zicovich-Wilson, C. M.; Pascale, F.; Roetti, C.; Saunders, V. R.; Orlando, R.; Dovesi, R. Calculation of the vibration frequencies of alpha-quartz: The effect of Hamiltonian and basis set. *J. Comput. Chem.* **2004,** *25*, 1873-1881.
31. Noel, Y.; D'Arco, P.; Demichelis, R.; Zicovich-Wilson, C. M.; Dovesi, R. On the Use of Symmetry in the Ab Initio Quantum Mechanical Simulation of Nanotubes and Related Materials. *J. Comput. Chem.* **2010,** *31*, 855-862.
32. Marana, N. L.; Albuquerque, A. R.; La Porta, F. A.; Longo, E.; Sambrano, J. R. Periodic density functional theory study of structural and electronic properties of single-walled zinc oxide and carbon nanotubes. *J. Solid State Chem.* **2016**, *237*, 36-47.
33. Marana, N. L.; Casassa, S. M.; Longo, E.; Sambrano, J. R. Structural, Electronic, Vibrational and Topological Analysis of Single-Walled Zinc Oxide Nanotubes. *J. Phys. Chem. C.* **2016**, *120*, 6814–6823 .
34. Vanduijneveldt, F. B.; Vanduijneveldtvanderijdt, J.; Vanlenthe, J. H. Statue-of-the-art in counterpoise theory. *Chem. Rev.* **1994,** *94*, 1873-1885.
35. Mayer, I.; Valiron, P. Second order Moller-Plesset perturbation theory without basis set superposition error. *J. Chem. Phys.* **1998,** *109*, 3360-3373.
36. Casarin, M.; Maccato, C.; Vittadini, A. A comparative study of the NH3 chemisorption on ZnO(1010) and Cu2O(111) non-polar surfaces. *Chem. Phys. Lett.* **1999,** *300*, 403-408.
37. Casarin, M.; Tondello, E.; Vittadini, A. A LCAO-LDF study of CO and NH3 chemisorption on ZnO(0001). *Surf. Sci.* **1994,** *307*, 1182-1187.
38. Casarin, M.; Tondello, E.; Vittadini, A. Coordination chemistry of CO and NH3 on ZnO(0001) - A molecular cluster study of the CO and NH3 bonding interaction with d10 ion. *Surf. Sci.* **1994,** *303*, 125-138.
39. Martins, J. B. L.; Longo, E.; Salmon, O. D. R.; Espinoza, V. A. A.; Taft, C. A. The interaction of H-2, CO, CO2, H2O and NH3 on ZnO surfaces: an Oniom Study. *Chem. Phys. Lett.* **2004,** *400*, 481-486.
40. Morimoto, T.; Yanal, H.; Nagao, M. Infrared spectra of ammonia adsorbed on zinc oxide. *J. Phys. Chem.* **1976,** *80*, 471-475.

41. Alecu, I. M.; Zheng, J. J.; Zhao, Y.; Truhlar, D. G. Computational Thermochemistry: Scale Factor Databases and Scale Factors for Vibrational Frequencies Obtained from Electronic Model Chemistries. *J. Chem. Theory Comput.* **2010,** *6*, 2872-2887.
42. Gatti, C. Chemical bonding in crystals: new directions. *Zeitschrift für Kristallographie - Cryst. Mat.*. **2009,** *220*, 399–457.

Figure Captions

Figure 1: NH_3 adsorption on various surface sites and with different coverages (a) (1) Model A – Zn_{Ax}-NH_3, (2) Model B – Zn_{Eq}-NH_3, (3) Model C – O-HNH_2, (4) Model D – O-HNH_2, and simultaneous adsorption (b) (5) both Zn_{Eq}, (6) Zn_{Eq} and Zn_{Ax}, and (7) both Zn_{Ax}

Figure 2: Nanotube deformation after NH_3 adsorption and optimization (a) 1-row of NH_3 molecules, (b) 2-rows (c) 4-rows NH_3, (d) 5-rows and (e) 10-rows.

Figure 3: Density of states (a) bare (10, 10) nanotube and (b) with 10-rows of NH_3 molecules adsorbed.

Figure 4: Infrared spectra of NH_3 adsorption on ZnONT in the low (a) and high (b) frequency range. In (c) a zoom of the peaks corresponding to the Zn-N stretching modes.

Figure 5: ZnO nanotube with NH_3 molecules adsorbed. In yellow, the atoms that were considered for the topological analysis in Table 3

Figure 06: (a) Electron density and (b) Laplacian of the electron density in the plane containing the N-Zn-O atoms evaluated at the B3LYP level. A logarithmic scale is adopted between -0.1 and 0.1 au. Continuous red and dotted blue lines indicate positive and negative contour levels, respectively.

Figure 1

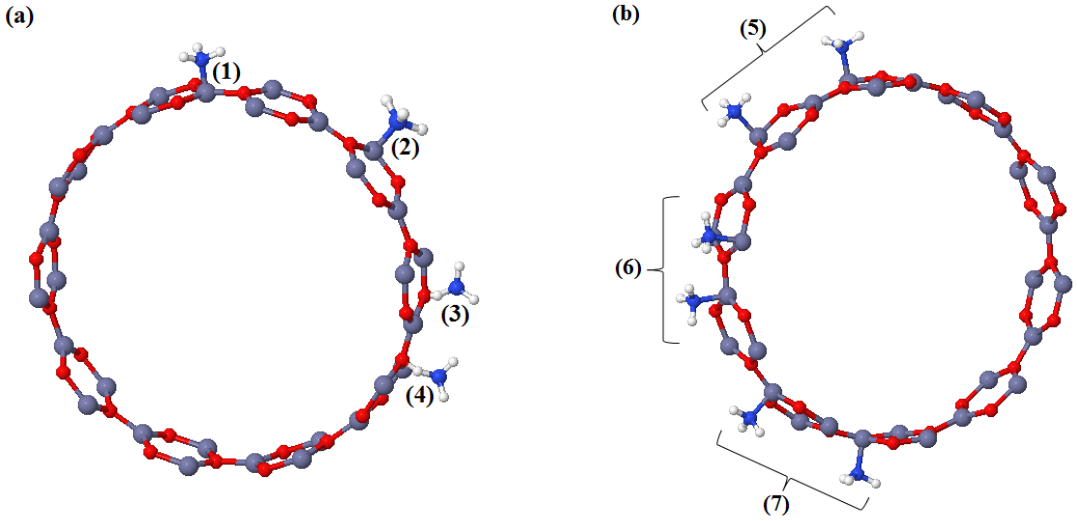

Figure 2

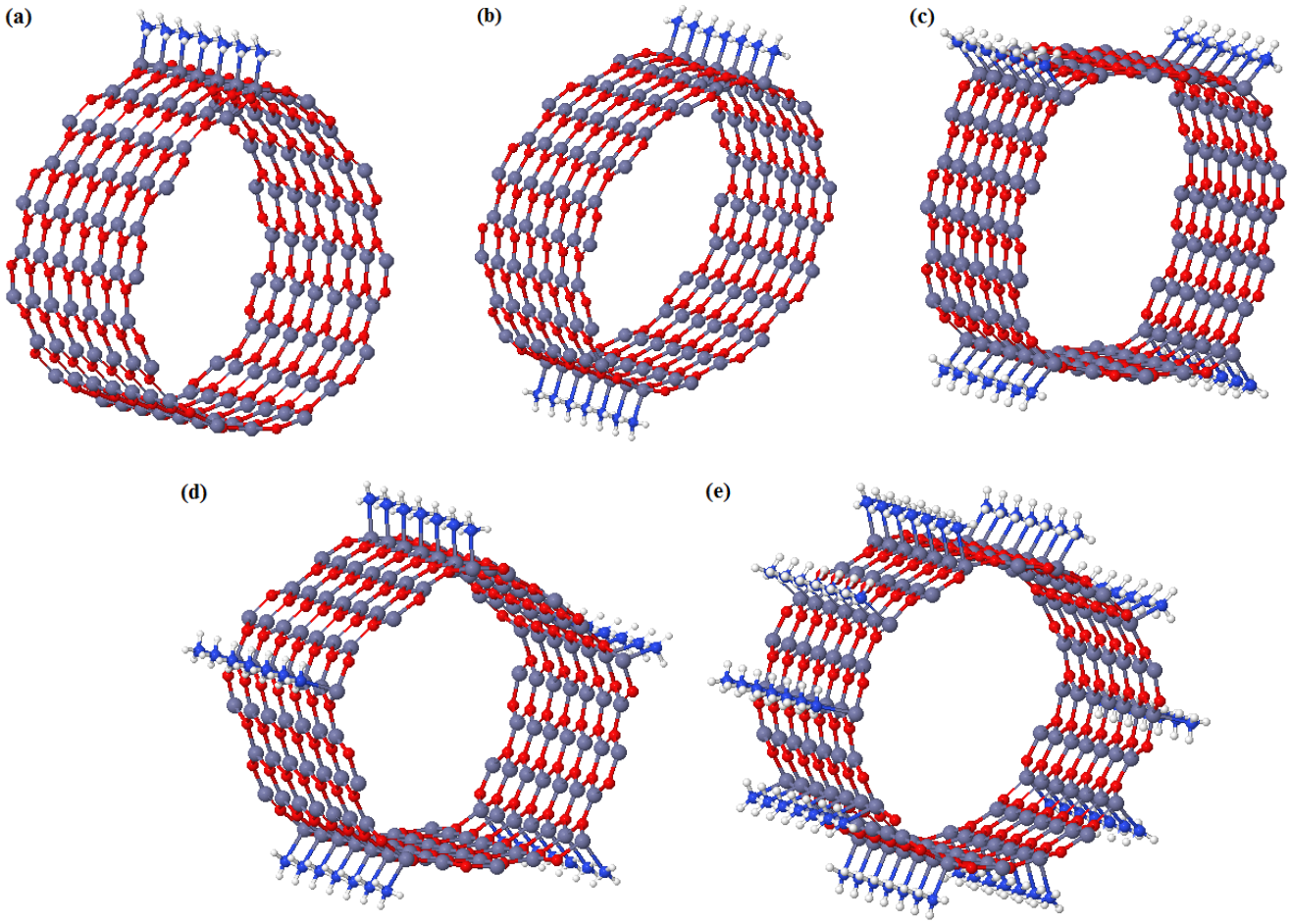

Figure 3

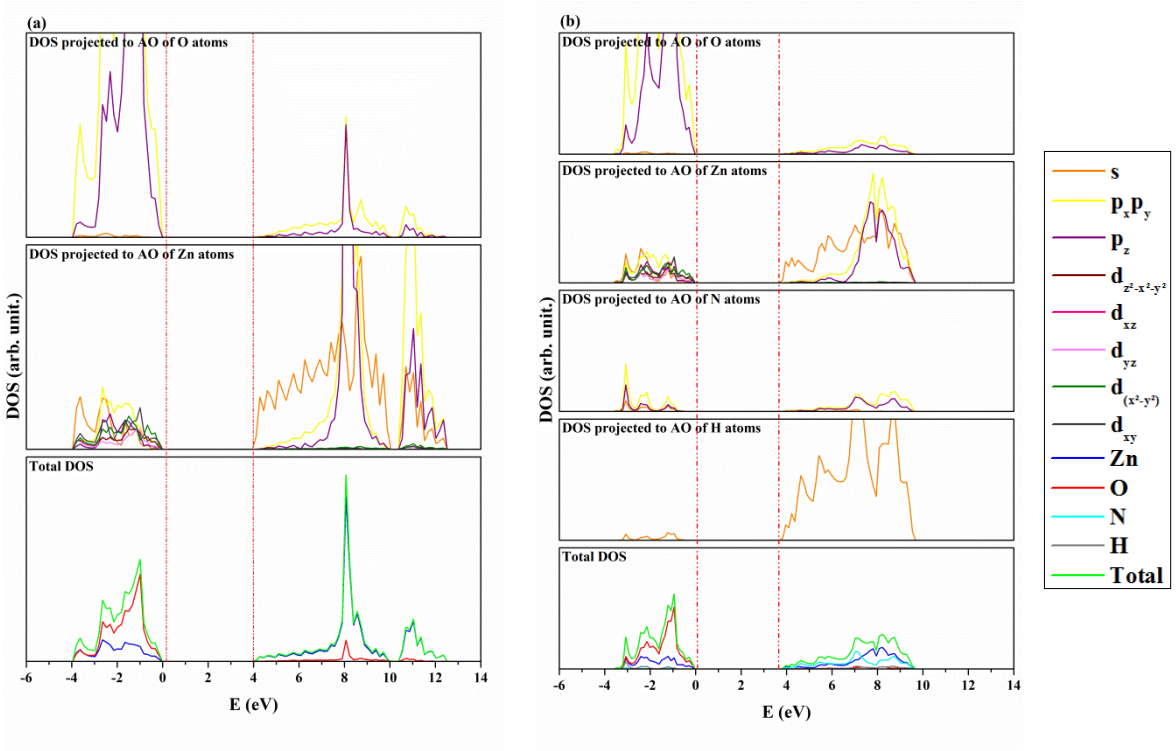
(a)
DOS projected to AO of O atoms
DOS projected to AO of Zn atoms
Total DOS
DOS (arb. unit.)
E (eV)
(b)
DOS projected to AO of O atoms
DOS projected to AO of Zn atoms
DOS projected to AO of N atoms
DOS projected to AO of H atoms
Total DOS
DOS (arb. unit.)
E (eV)
s
$p_x p_y$
p_z
$d_{z^2-x^2-y^2}$
d_{xz}
d_{yz}
$d_{(x^2-y^2)}$
d_{xy}
Zn
O
N
H
Total

Figure 4

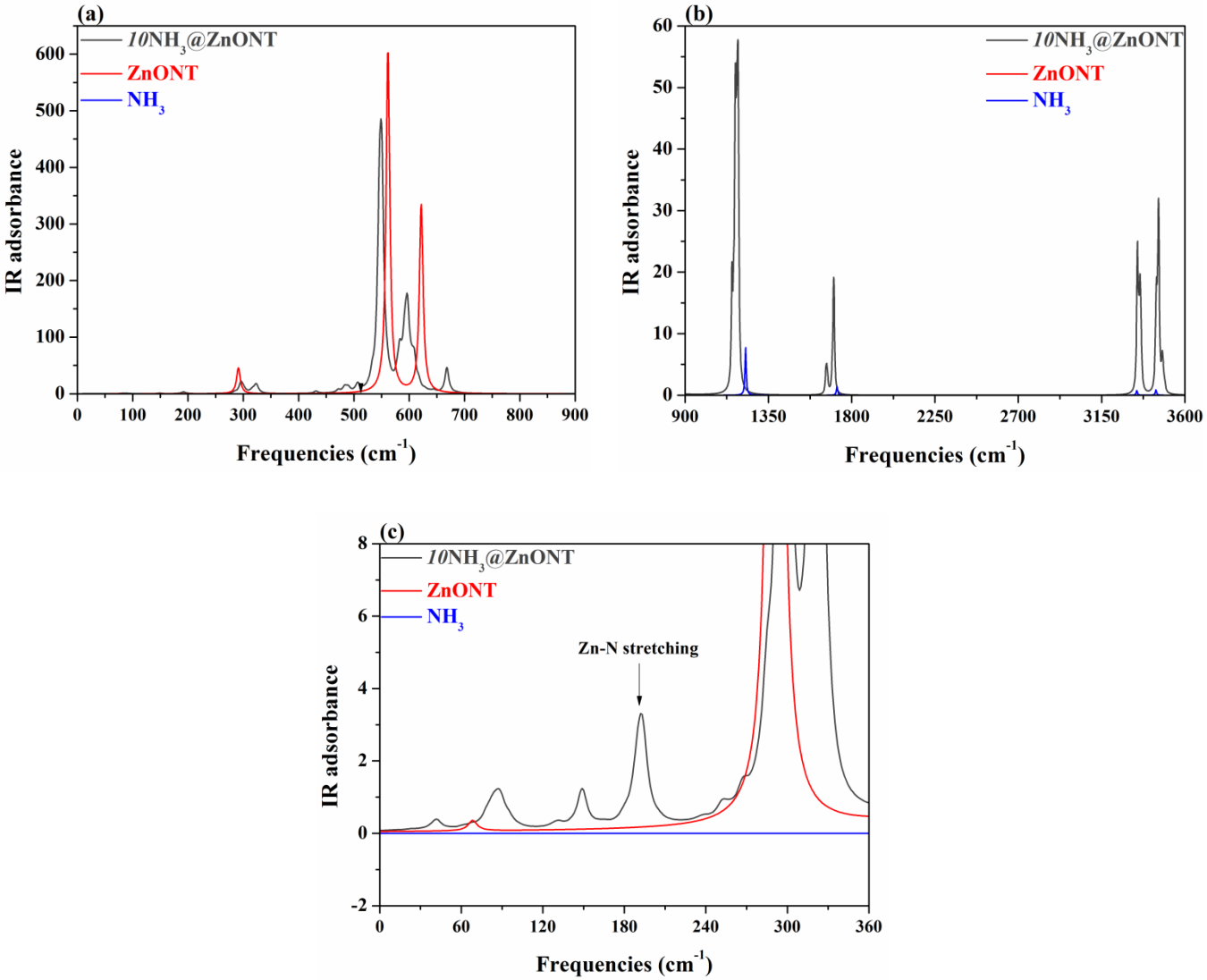
(a)
10NH3@ZnONT
ZnONT
NH3
IR adsorbance
Frequencies (cm-1)
(b)
10NH3@ZnONT
ZnONT
NH3
IR adsorbance
Frequencies (cm-1)
(c)
10NH3@ZnONT
ZnONT
NH3
Zn-N stretching
IR adsorbance
Frequencies (cm-1)

Figure 5

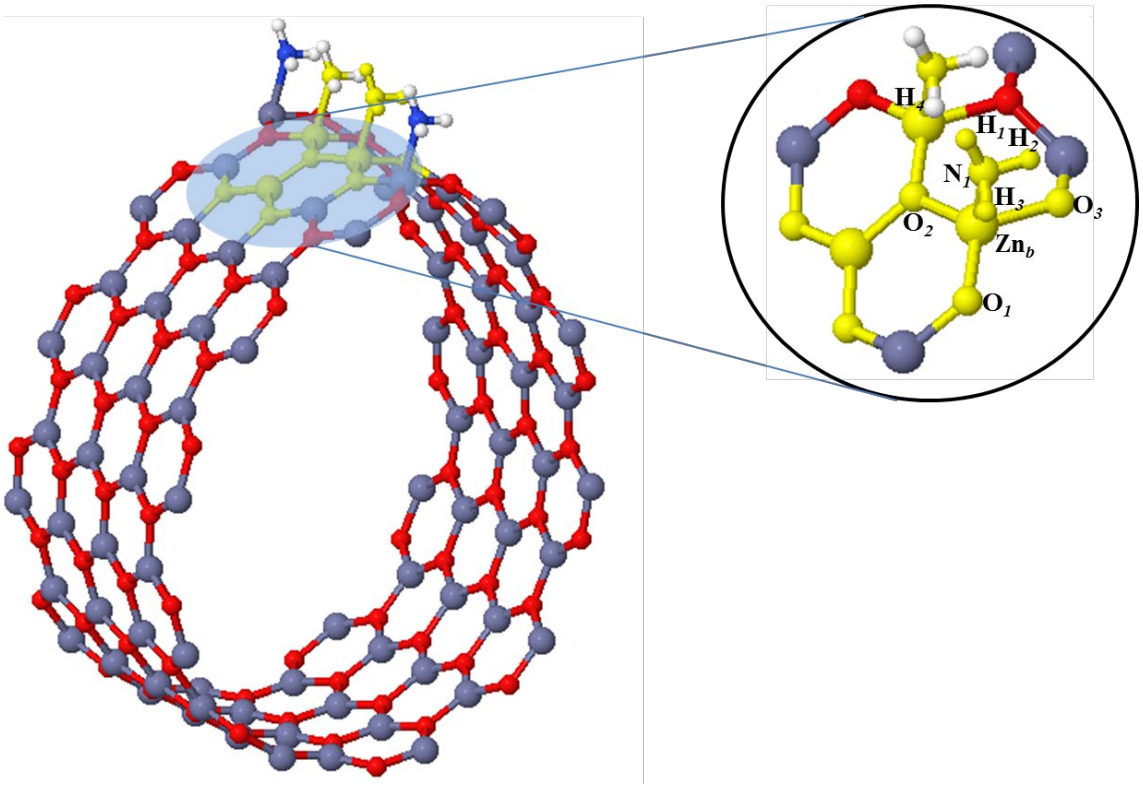

Figure 6

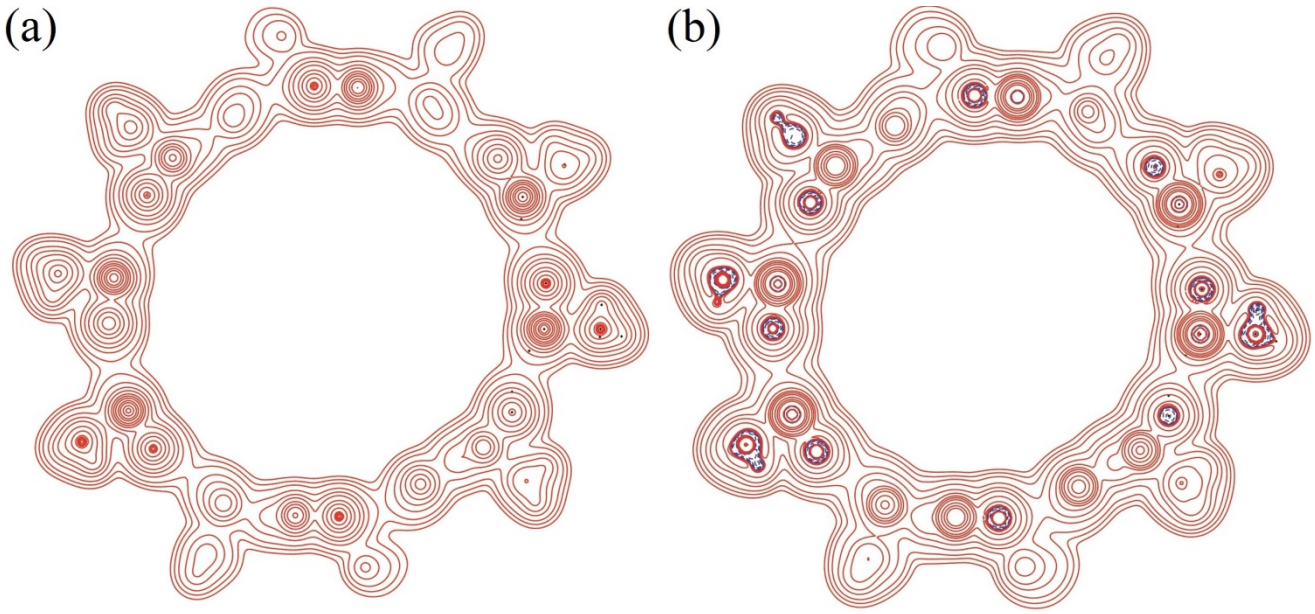

Table Captions

Table 1: Zn-O, N-H, and Zn-N bond lengths (Å), Zn-O-Zn and H-N-H bond angles (degree) distortion energy (E_{dist}) and adsorption energy (E_{ads}) in kcal/mol and band gap ($E_{gap,}$ eV) of *n*NH3@ZnONT. The sub-index *s* refers to the atoms of the adsorption site.

Table 2: Adsorption energies and enthalpy at 0 and 298 K in kcal/mol

Table 3: Topological properties at the bond critical points (electron charge density ($\rho(r)$), Laplacian ($\nabla^2\rho$), |V|/G ratio, bond degree H/ρ(r), ellipticity ε) plus Bader charges and atomic volumes (all in atomic units) are computed for the atoms involved in the physisorption (labels of atoms as in Figure 5). Subindex *f* refers to the isolated nanotube and NH_3; *t*, *cov* and *H-bond* refers to the transit, covalent and hydrogen bond type

Table 1

nNH$_3$	d_{Zn-O}	$d_{s(Zn-O)}$	$\alpha_{Zn-O-Zn}$	$\alpha_{sZn-O-Zn}$	d_{Zn-N}	d_{N-H}	α_{H-N-H}	E_{dist}	E_{ads}	$E_{ads}+E_{BSSE}$	E_{gap}
0	1.89	1.89	119.79	119.79	-	-	-	-	-	-	4.52
1	1.89	1.93	119.88	116.12	2.32	1.02	107.49	3.35	-16.77	-4.46	4.18
1-row	1.91	1.94	119.74	117.88	2.32	1.02	103.02	2.45	-9.70	-5.46	4.36
2-row	1.90	1.94	119.64	117.87	2.30	1.02	107.35	5.39	-14.38	-4.95	4.43
4-row	1.90	1.94	119.87	118.17	2.31	1.02	107.30	3.72	-15.79	-6.43	4.38
5-row	1.90	1.94	119.90	118.28	2.33	1.02	106.40	3.50	-15.84	-6.48	4.37
10-row	1.90	1.93	119.90	118.93	2.37	1.02	106.33	2.14	-15.46	-6.31	4.22
6^{11} (6,0)	1.94	-	-	-	2.16	-	-	-	-18.86	-	2.25
1^{37} (0001)	-	-	-	-	2.04	-	-	-	-51.00	-	-
1^{36} ($10\bar{1}0$)	-	-	-	-	2.06	1.02	107.00	-	-35.00	-	-
1^{39} ($10\bar{1}0$)	-	-	-	-	2.06	1.01	-	-	-42.02	-	-

Table 2

nNH$_3$	E_{ads}+ E_{BSSE}	H_{ads} (0K)	H_{ads} (298K)
1-row	-5.46	-3.30	-2.84
4-row	-6.43	-4.30	-4.21
10-row	-6.31	-4.31	-4.28

Table 3

	Bond Critical Points								Atomic Properties	
	$d_{BCP-Zn/N}$	$d_{BCP-O/H}$	$\rho(r)$	$\nabla^2\rho$	|V|/G	H/$\rho(r)$	ε	*bond*	Q	V
Zn_f									1.27	79.80
O_{in}	0.919	0.970	0.098	0.571	1.06	-0.09	0.028	*t*	-1.12	112.67
O_{out}	0.920	0.971	0.090	0.508	1.05	-0.08	0.028	*t*	-1.20	111.58
N_f									-0.84	94.36
H_f	0.747	0.279	0.320	-1.359	8.36	-1.23	0.037	*cov*	0.28	38.83
1-row NH_3										
Zn_b									1.29	78.93
O_1	0.922	0.975	0.098	0.573	1.06	-0.09	0.026	*t*	-1.11	111.82
O_2	0.972	0.983	0.095	0.551	1.06	-0.09	0.025	*t*	-1.19	111.38
O_3	0.941	1.004	0.088	0.489	1.05	-0.08	0.011	*t*	-1.04	108.96
N_1	1.104	1.197	0.043	0.121	1.23	-0.21	0.034	*t*	-1.08	111.84
N_1									-1.08	112.83
H_1	0.748	0.279	0.323	-1.413	9.01	-1.25	0.028	*cov*	0.34	32.40
H_2	0.756	0.267	0.323	-1.454	9.73	-1.27	0.027	*cov*	0.38	29.90
H_3	0.760	0.263	0.323	-1.472	9.97	-1.28	0.025	*cov*	0.40	23.11
H_4	1.479	0.880	0.013	0.045	0.91	0.07	0.193	*H-bond*	0.38	37.71
10-row NH_3										
Zn_b									1.29	80.58
O_1	0.928	0.984	0.094	0.547	1.06	-0.09	0.021	*t*	-1.12	112.94
O_2	0.923	0.976	0.097	0.569	1.06	-0,09	0,023	*t*	-1.20	111.38
O_3	0.936	0.997	0.090	0.509	1.05	-0.08	0.013	*t*	-1.04	108.98
N_1	1.146	1.236	0.036	0.095	1.25	-0.22	0.041	*t*	-1.08	114.03
N_1									-1.08	114.03
H_1	0.746	0.276	0.323	1.391	8.71	-1.24	0.030	*cov*	0.33	33.44
H_2	0.762	0.264	0.321	1.457	9.94	-1.28	0.026	*cov*	0.40	23.36
H_3	0.755	0.268	0.323	1.440	9.52	-1.26	0.028	*cov*	0.37	30.51
H_4	1.495	0.892	0.013	0.043	0.91	0.07	0.156	*H-bond*	0.36	38.26